UNDERWATER IMAGE RESTORATION BASED ON MINIMUM INFORMATION LOSS PRINCIPLE AND OPTICAL PROPERTIES OF UNDERWATER IMAGING

Chongyi Li[1], *Jichang Guo*[1], *Shanji Chen*[2], *Yibin Tang*[3], *Yanwei Pang*[1], *Jian Wang*[1,4]

[1]Tianjin University, School of Electronic Information Engineering
[2]Qinghai Nationalities University, College of Physics and Electronic Information Engineering
[3]Hohai University, College of Internet of Things Engineering
[4]National Ocean Technology Center
E-mail: lichongyi@tju.edu.cn

ABSTRACT

Restoring underwater image from a single image is known to be an ill-posed problem. Some assumptions made in previous methods are not suitable in many situations. In this paper, an effective method is proposed to restore underwater images. Using the quad-tree subdivision and graph-based segmentation, the global background light can be robustly estimated. The medium transmission map is estimated based on minimum information loss principle and optical properties of underwater imaging. Qualitative experiments show that our results are characterized by relatively genuine color, natural appearance, and improved contrast and visibility. Quantitative comparisons demonstrate that the proposed method can achieve better quality of underwater images when compared with several other methods.

Index Terms— Underwater image restoration, underwater image enhancement, image dehazing, image degradation, visibility recovery

1. INTRODUCTION

Underwater imaging is widely used in scientific research and technology due to the low cost of implementation when compared with more sophisticated techniques. However, underwater imaging is still challenging due to the physical properties of underwater conditions. An underwater image can be represented as a linear superposition of a direct component, a forward scattering component, and a back scattering component [1]. Such a light absorption attenuates energy of the direct light, degrades contrast, and causes a hazy image background. Meanwhile, such a forward scattering causes the blurring of the image features whereas the back scattering masks the details of the scenario. In the water, the natural illumination also undergoes a strong color-dependent attenuation. As a result, underwater images generally have predominantly green-blue hue. The overall poor visibility and color cast caused by the effects of underwater imaging conditions deteriorate the capability to fully extract valuable information from underwater images for further processing such as marine mine detection and aquatic robot inspection. Hence, it is of great interest to restore degraded underwater images for high-quality underwater imaging.

Numerous underwater image restoration and enhancement methods have emerged in recent years. Carlevaris-Bianco *et al.* [2] proposed a simple yet effective prior that exploits the strong difference in attenuation among the three color channels in the water to estimate the depths of the scene. Chiang and Chen [3] restored underwater images by combining a dehazing algorithm with wavelength compensation. The effects of the haze from light scattering can be removed by the classical dark channel prior algorithm [4]. According to the amount of attenuation of each wavelength, reverse compensation is conducted to restore the distortion from color cast. Ancuti *et al.* [5] enhanced the visual quality of underwater images and videos based on the fusion principle. Galdran *et al.* [6] proposed a red channel method, where the lost contrast and color associated with short wavelength are recovered. Besides, multiple images [7] and specialized devices [8] are employed to enhance underwater images.

In this paper, we develop a method for underwater image restoration that includes two processing steps: global background light estimation and medium transmission map estimation. The contributions of this work are summarized as follows: 1) it introduces a robust global background light estimation algorithm based on quad-tree subdivision and graph-based segmentation; 2) it presents a new medium transmission map estimation algorithm via minimizing information loss and deriving imaging optical properties; 3) it is parameter-free, which avoids manual parameter tuning. The rest of the paper is organized as follows: Section 2 describes the proposed method. Section 3 evaluates and compares the

This work was supported by the National Key Basic Research Program of China (2014CB340403) the Natural Science Foundation of Qinghai Province of China (2015-ZJ-721), and the Specialized Research Fund for the Doctoral Program of Higher Education (20120032110034).

experimental results. Section 4 concludes this paper.

2. PROPOSED METHOD

The simplified underwater optical imaging model can be described as:

$$I^c(x) = J^c(x)t^c(x) + A^c(1 - t^c(x)), c \in \{r, g, b\}, \quad (1)$$

where *x* denotes a pixel, *I(x)* is the degraded image, *J(x)* is the restored image, *A* is the global background light, and *t(x)*∈ [0,1] is the medium transmission map. The purpose of image restoration is to recover *J(x)* from *I(x)*. As only *I(x)* is available, we need to estimate both *A* and *t(x)* simultaneously.

2.1. Global Background Light Estimation

The global background light is often estimated as the brightest color in an underwater image. However, the assumption is not true in such a scheme where objects are brighter than the global background light. To robustly estimate the global background light, we employ a hierarchical searching method based on the quad-tree subdivision [9], and then segment background regions using a graph-based segmentation [10]. An example to illustrate the proposed global background light estimation is presented in Fig. 1.

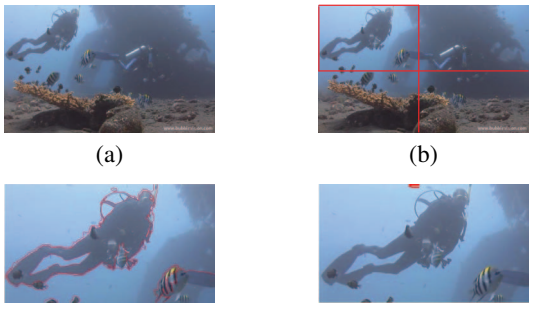

Fig. 1. An example of the global background light estimation. (a) Raw underwater image. (b) Result of quad-tree subdivision, where red rectangle represents the candidate region. (c) Result of graph-based segmentation, where red line indicates the boundary between background and foreground. (d) Result of searching for the brightest pixels in dark channel, where red pixels denote the candidates of global background light.

The details are illustrated as follows. An input image is divided into four rectangular regions by using quad-tree division algorithm. The score of each region is defined as the average pixel value subtracted by the standard deviation of the pixel values within the region. The region with highest score is selected as the candidate region in order to select flat background region. Then the background of the candidate region is segmented by a graph-based segmentation algorithm for removing the effect of front objects. In the graph-based segmentation algorithm, texture and color features are applied to distinguish background and foreground. The size of the initial segmentation is set to 250. The other parameters in the graph-based segmentation algorithm are set by default. To avoid the effects of suspended particles, we pick up the top 0.1 percent brightest pixels in the dark channel of the segmented background region [4]. According to the characteristic of underwater optical imaging, the blue light travels the longest in the water because of its shortest wavelength, followed by the green light and then the red light. Finally, among the above-selected brightest pixels, the pixel with the maximum blue-red difference in the input image is regarded as the estimated global background light for guaranteeing the robustness of the proposed algorithm. More results can be seen in Fig. 2.

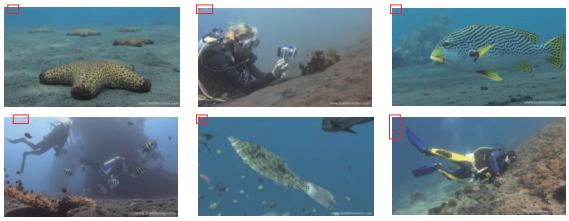

Fig. 2. Results of the proposed global background light estimation algorithm. Red pixels in the red rectangle represent the candidates of the estimated global background light.

2.2. Medium Transmission Map Estimation

According to the Lambert-Beer empirical law [11], the medium transmission map can be expressed as:

$$t^c(x) = \exp(-p^c d(x)), c \in \{r, g, b\}, \quad (2)$$

where *d(x)* is the distance from the scene point to the camera, p^c is the total attenuation coefficient, which can be decomposed as a linear superposition of absorption coefficient a^c and scattering coefficient b^c. b^c is the superposition of all scattering events at all angles, and can be expressed as:

$$b^c = \int_0^\pi \beta^c(\omega)\, \mathrm{d}\omega = 2\pi \int_0^\pi \beta^c(\theta) \sin\theta\, \mathrm{d}\theta, \quad (3)$$

where $\beta^c(\theta)$ is the integral of the volume scattering function over all solid angles. According to (1), the medium transmission function can be written as:

$$J^c(x) = \frac{1}{t^c(x)}(I^c(x) - A^c) + A^c. \quad (4)$$

An example of the medium transmission function in (4) is shown in Fig. 3. As shown in Fig. 3, input values in $[\alpha, \beta]$ are mapped to output values in the full dynamic range [0, 255],

where the medium transmission map t^c determines the valid input range $[\alpha, \beta]$. When some input values lie outside of the range $[\alpha, \beta]$, the mapped output values do not belong to the valid output range [0, 255]. In such cases, the underflow or overflow occurs in some pixel values, which are truncated to 0 or 255. The truncated pixel values mean information loss and can be seen in the red regions in Fig. 3.

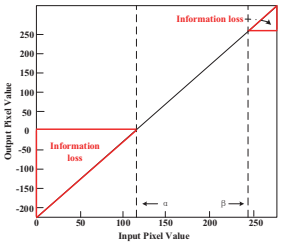

Fig. 3. An example of the medium transformation function. Input pixel values are mapped to output pixel values according to the medium transformation function, depicted by the black line. The red regions denote the information loss due to the truncation of output pixel values.

To reduce the information loss, we impose a constraint to the medium transmission map such that the restored image is still in the range [0, 255] [9]. From our analysis and observations, we define an information loss cost in a local block B for red channel:

$$\begin{aligned} Infor_{loss} = \sum_{x\in B}\{(\min(0, \frac{I^r - A^r}{t^r} + A^r))^2 \\ + (\max(0, \frac{I^r - A^r}{t^r} + A^r - 255))^2\}. \end{aligned} \tag{5}$$

In order not to yield any information loss, (5) should satisfy the following constraint:

$$\begin{cases} \min\limits_{x\in B}(\frac{I^r(x)-A^r}{t^r} + A^r) \geq 0 \\ \max\limits_{x\in B}(\frac{I^r(x)-A^r}{t^r} + A^r - 255) \leq 0. \end{cases} \tag{6}$$

Assuming that the medium transmission map in a local block has the same pixel value, the estimated medium transmission map t^{r^*} can be obtained by combining (4) and (6):

$$t^{r^*} \geq \max[\min_{x\in B}(\frac{I^r(x) - A^r}{-A^r}), \max_{x\in B}(\frac{I^r(x) - A^r}{255 - A^r})]. \tag{7}$$

In this paper, we select the smallest value, which satisfies the constraint in (7). Experiments found that the larger medium transmission map may cause contrast cost. After obtaining the crude medium transmission map block-by-block, we incorporate the guided filter [12] to refine it for removing the blocking artifacts. The refined result is shown in Fig. 4.

Next, we estimate the medium transmission maps of the green and blue channels by exploring the correlation between

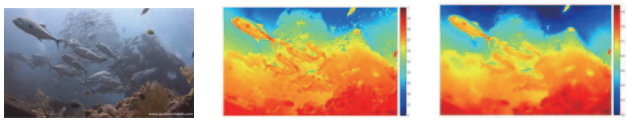

(a) (b) (c)

Fig. 4. The medium transmission map of red channel. (a) Raw underwater image. (b) The coarse medium transmission map. (c) The refined medium transmission map. In the medium transmission map, the color bar represents different pixel values.

the medium transmission map and optical properties of underwater imaging. Inspired by [13], the total background light from the scene point to the camera can be obtained by integrating the attenuation from distance *l=0* to *l=d* and casting up all scattering components at all directions. The total background light $L^c(d)$ can be expressed as:

$$\begin{aligned} L^c(d) &= \int_0^d \int_\theta \beta^c(\varphi) E_a \exp(-p^c l) k_l \, \mathrm{d}l \, \mathrm{d}\varphi \\ &= A^c(\infty)[1 - \exp(-p^c d)], \end{aligned} \tag{8}$$

where θ denotes all possible scattering angles for a certain scattering volume, $\beta^c(\theta)$ is the volume scattering function, E_a is the intensity of the ambient light and simplified to a constant, p^c is the total attenuation coefficient, k_l represents the properties of camera system and is a constant within a single image, and

$$A^c(\infty) = \frac{k_l E_a}{p^c} \int_\theta \beta^c(\varphi) \, \mathrm{d}\varphi, \tag{9}$$

where $A^c(\infty)$ is the global background light, $\int_\theta \beta^c(\varphi) \, \mathrm{d}\varphi$ denotes scattering events toward the camera from all directions, and is essentially identical with the definition of scattering coefficient b^c in (3). $A^c(\infty)$ can be rewritten as:

$$A^c(\infty) \propto \frac{b^c}{p^c}. \tag{10}$$

Besides, Gould *et al.* [14] found scattering coefficient has an approximate linear relationship with light wavelength in general water, and can be expressed as:

$$b^c = (-0.00113\lambda_c + 1.62517) b(555nm), \tag{11}$$

where λ_r, λ_g, and λ_b are 620nm, 540nm, and 450nm in general water, respectively. $b(555nm)$ is a scattering coefficient at a particular wavelength of light [14]. According to (10) and (11), ratios of the total attenuation coefficient can be expressed as:

$$\frac{p^c}{p^r} = \frac{b^c B^r(\infty)}{b^r B^c(\infty)}, c \in \{g, b\}, \tag{12}$$

where p^g/p^r and p^b/p^r are the green-red total attenuation coefficient ratio and blue-red total attenuation coefficient ratio, respectively. According to (2), the medium transmission map has an exponential correlation with the total attenuation coefficient. Therefore, the medium transmission maps of the green and blue channels can be expressed as:

$$t^c(x) = (t^r(x))^{\frac{p^c}{p^r}}, c \in \{g, b\}, \tag{13}$$

Finally, the degraded underwater image can be restored according to (4). Based on the observation that the dark or bright regions in underwater images become too dark or too bright after being restored, an adaptive exposure map [15] is employed to adjust our results for better visual quality.

3. EXPERIMENTAL RESULTS

To evaluate the performance of the proposed method, qualitative and quantitative comparisons are carried out, respectively. The methods used for comparisons include traditional image enhancement method (e.g., Histogram Equalization (HE)), Chromatism-based [2] underwater image enhancement method (CB), and classical image dehazing method (e.g., Dark Channel Prior (DCP) [4]).

3.1. Qualitative Comparison

As shown in Fig. 5, our method has successfully restored the contrast, relatively genuine color, and visibility of the raw underwater images. Moreover, the appearance of our result is neither over-enhanced nor under-enhanced. HE method introduces artifacts due to ignoring the spatially varying distance dependencies. Although the contrast and details are increased by DCP and CB methods, the colors and visibility are poor because the attenuated energy is not compensated individually based on different wavelengths. Furthermore, we attempt to process raw underwater image taken in challenging scenes (i.e., artificial lighting scene and turbid scene). Challenging scenes comparison in Fig. 6 shows that our result are more natural and visible and have fewer artifacts than the results of the compared methods.

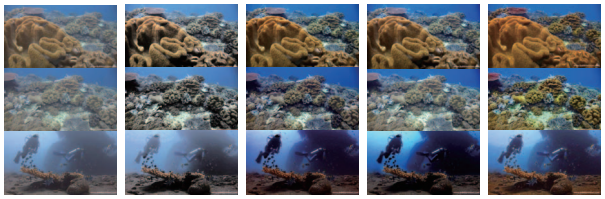

(a) (b) (c) (d) (e)

Fig. 5. Qualitative comparison. (a) Raw underwater images. (b) HE. (c) DCP. (d) CB. (e) Our method.

(a) (b) (c) (d) (e)

Fig. 6. Qualitative comparison on challenging scenes. (a) Top: image captured in turbid underwater scene, bottom: image captured with artificial lighting). (b) HE. (c) DCP. (d) CB. (e) Our method.

3.2. Quantitative Comparison

Following other researchers, entropy, patch-based contrast quality index (PCQI) [16], and underwater color image quality evaluation (UCIQE) metric [17] are employed to evaluate the performance of the proposed method. To quantify the performance of the different methods, we extracted 500 images from a video *(http:// www.youtube.com/user/bubblevison)* which is also used by previous work. Some of these images are shown in Fig. 2 and Fig. 5. Table 1 summarizes the average values of the entropy, PCQI, and UCIQE. The values in bold represent the best results.

Table 1. Quantitative Results

Method	Entropy	PCQI	UCIQE
HE	7.6807	**1.0491**	0.5161
DCP	6.7641	0.9213	0.4610
CB	6.3434	0.5839	0.5198
Our	**7.7556**	1.0310	**0.6013**

Table 1 shows that our method outperforms other methods in terms of the values of entropy and UCIQE. The higher entropy values indicate that our method can sufficiently reduce information loss of restoring the degraded underwater images and increase the valuable information. The higher UCIQE score means that our method can well balance the chroma, saturation, and contrast of the restored underwater images. The higher PCQI values indicate the results have most contrast changes. Our method ranks second in terms of PCQI evaluation. Further experiments found that the highest PCQI value produced by HE method may result from the enhanced noise.

4. CONCLUSION

In this work, we develop a physics-based method for recovery of visibility and colors of the degraded underwater images based on minimum information loss principle and optical properties of underwater imaging. Experimental results show that the proposed method can well handle underwater images, even for the images captured in the challenging underwater scenes.

5. REFERENCES

[1] R. Schettini and S. Corchs, "Underwater image processing: state of the art of restoration and image enhancement methods," *EURASIP Journal on Advances in Signal Processing*, vol. 2010, pp. 1–14, 2010.

[2] N. Carlevaris-Bianco, A. Mohan, and R. M. Eustice, "Initial results in underwater single image dehazing," in *Processing of IEEE Conference on OCEANS*, 2010, pp. 1–8.

[3] J. Y. Chiang and Y. C. Chen, "Underwater image enhancement by wavelength compensation and dehazing," *IEEE Transactions on Image Processing*, vol. 21, pp. 1756–1769, 2012.

[4] K. He, J. Sun, and X. Tang, "Single image haze removal using dark channel prior," *IEEE Transactions on Pattern Analysis and Machine Intelligence*, vol. 33, pp. 2341–2353, 2011.

[5] C. Ancuti, C. O. Ancuti, T. Haber, and P. Bekaert, "Enhancing underwater images and videos by fusion," in *Processing of IEEE Conference on Computer Vision and Pattern Recognition*, 2012, pp. 81–88.

[6] A. Galdran, D. Pardo, A. Picón, and A. Alvarez-Gila, "Automatic red-channel underwater image restoration," *Journal of Visual Communication and Image Representation*, vol. 26, pp. 132–145, 2015.

[7] Y. Schechner, Y. Yoav, and Y. Averbuch, "Regularized image recovery in scattering media," *IEEE Transactions on Pattern Analysis and Machine Intelligence*, vol. 29, pp. 1655–1660, 2007.

[8] B. Ouyang, F. Dalgleish, and et al. A. Vuorenkoski, "Visualization and image enhancement for multistatic underwater laser line scan system using image-based rendering," *IEEE Journal of Oceanic Engineering*, vol. 38, pp. 566–580, 2013.

[9] J. Kim, W. Jang, and et al. J. Sim, "Optimized contrast enhancement for real-time image and video dehazing," *Journal of Visual Communication and Image Representation*, vol. 24, pp. 410–425, 2013.

[10] P. Felzenszwalb, F. Pedro, and D. Huttenlocher, "Efficient graph-based image segmentation," *International Journal of Computer Vision*, vol. 59, pp. 167–181, 2004.

[11] H. Gordon, "Can the lambert-beer law be applied to the diffuse attenuation coefficient of ocean water?," *Limnology and Oceanography*, vol. 34, pp. 1389–1409, 1989.

[12] K. He, J. Sun, and X. Tang, "Guided image filtering," *IEEE Transactions on Pattern Analysis and Machine Intelligence*, vol. 35, pp. 1397–1409, 2013.

[13] Y. Schechner, Y. Yoav, and N. Karpel, "Clear underwater vision," in *Processing of IEEE Conference on Computer Vision and Pattern Recognition*, 2004, pp. 536–543.

[14] R. Gould, R. Arnone, and P. Martinolich, "Spectral dependence of the scattering coefficient in case 1 and case 2 waters," *Applied Optics*, vol. 38, pp. 2377–2383, 1999.

[15] K. Tang, J. Yang, and J. Wang, "Investigating haze-relevant features in a learning framework for image dehazing," in *Processing of IEEE Conference on Computer Vision and Pattern Recognition*, 2014, pp. 2995–3002.

[16] S. Wang, K. Ma, and et al. H. Yeganeh, "A patch-structure representation method for quality assessment of contrast changed images," *IEEE Signal Processing Letters*, vol. 22, pp. 2387–2390, 2015.

[17] M. Yang and A. Sowmya, "An underwater color image quality evaluation metric," *IEEE Transactions on Image Processing*, vol. 24, pp. 6062–6071, 2015.